LAWRENCE
LIVERMORE
NATIONAL
LABORATORY

LLNL-JRNL-669760

Blue Light Emission from Cyclometallated Iridium (III) Cyano Complexes: Syntheses, Crystal Structures, and Photophysical Properties

R. D. Sanner, N. J. Cherepy, V. G. Young

April 16, 2015

Inorganica Chimica Acta

Disclaimer

Blue Light Emission from Cyclometallated Iridium (III) Cyano Complexes: Syntheses, Crystal Structures, and Photophysical Properties

Robert D. Sanner and Nerine J. Cherepy*
Lawrence Livermore National Laboratory, Livermore, CA 94550

Victor G. Young, Jr.
Department of Chemistry, University of Minnesota, Minneapolis, MN 55455

Abstract

We describe the synthesis and crystal structures of four iridium compounds containing the 2-(4,6-difluorophenyl)pyridyl ligand. Cleavage of dichloro-bridged iridium (III) dimers with phosphorus ligands leads to $(46dfppy)_2Ir(L)(Cl)$ where L = PPh_3 or $P(OPh)_3$. Treatment of the chloro compounds with cyanide forms the cyano complexes $(46dfppy)_2Ir(L)(CN)$. All complexes exhibit a trans effect in their molecular structures due to the phosphorus ligands, with the phosphite having a greater effect than the phosphine. With L = PPh_3, blue photoluminescence with CIE coordinates (x = 0.16, y = 0.24), quantum yield of 0.82 and 4.5 microsecond decay time is measured. For L = $P(OPh)_3$, blue photoluminescence with CIE coordinates (x = 0.16, y = 0.21), quantum yield of 0.81 and 2.9 microsecond decay time is measured.

Introduction

Cyclometalated iridium(III) complexes have been investigated in recent years as emissive materials for organic light-emitting diodes (OLEDs).[1] A common cyclometalating ligand is the 2-phenylpyridyl moiety (ppy) which has shown its usefulness in a host of compounds with widely varying emission characteristics. Representative examples display emission across the visible spectrum including red,[2] orange,[3] green,[4] and blue.[5]

To obtain the highest light yields in OLEDs[6] or in plastic scintillators,[7] at low doping levels, the lowest-lying triplet state of the iridium complex must lie at lower energy than the host. For example, N,N'-dicarbazolyl-3,5-benzene (mCP, T_1 = 2.9 eV) offers excellent efficiency with the best known blue-green iridium complex, bis[2-(4,6-difluorophenyl) pyridinato-C2,N](picolinato)iridium, $Ir(46dfppy)_2$(pic), or FIrpic (T_1 = 2.7 eV), at doping levels of ~1%.[8] A variety of deeper blue-emitting Iridium complexes have been reported, many with modest quantum yields, and some have limited stability under operating conditions in OLED devices.[5,6,8-11] For these reasons, alternative blue phosphorescent emitters, in particular, blue emitters with low-lying T_1 states for use in the full range of hosts, are of interest.

We have sought to prepare compounds with emission in the deep blue which can be realized by maximizing the HOMO-LUMO energy gap of the complex. Our approach is to focus on lowering the energy of the predominantly metal-centered t_{2g} HOMO while leaving the ligand-centered LUMO relatively unchanged. Thus, strong field electron-withdrawing ancillary ligands such as triphenylphosphine and cyanide merit investigation.[12] In addition to ancillary ligand effects, substitution of the phenyl hydrogens on the phenylpyridine

group has been shown to influence the HOMO-LUMO gap. The use of electron-withdrawing fluorine atoms, particularly at the 4 and 6 positions, stabilizes the HOMO more than the LUMO and causes a blue shift in emission.[13,14] Prior workers have reported the use of the difluorophenylpyridyl ligand with an ancillary phosphine ligand as in $Ir(46dfppy)_2(PPh_3)(L)$, where 46dfppy=2-(4,6-difluorophenyl)pyridyl and L=(NCS^-) or (NCO^-).[9] Also, phosphine complexes using nonfluorinated phenylpyridine ligands are known, as in $Ir(ppy)_2(PPh_3)(L)$, where L=(NCS^-), (N_3^-), or (NCO^-)[15] and $Ir(ppy)_2(L)(CN)$, where L=PPh_3, P(*n*-Bu)$_3$, or $P(OPh)_3$.[16] We report herein the synthesis, x-ray structural characterization, and electronic spectroscopy of four compounds: $(46dfppy)_2Ir(PPh_3)(X)$ and $(46dfppy)_2Ir[P(OPh)_3](X)$, where X=($Cl^-$) or ($CN^-$). We examine the differences in the steric and electronic properties of the two phosphorus ligands[17] and their influence on the structures and emission spectra of the complexes.

Scheme 1. Synthetic procedures

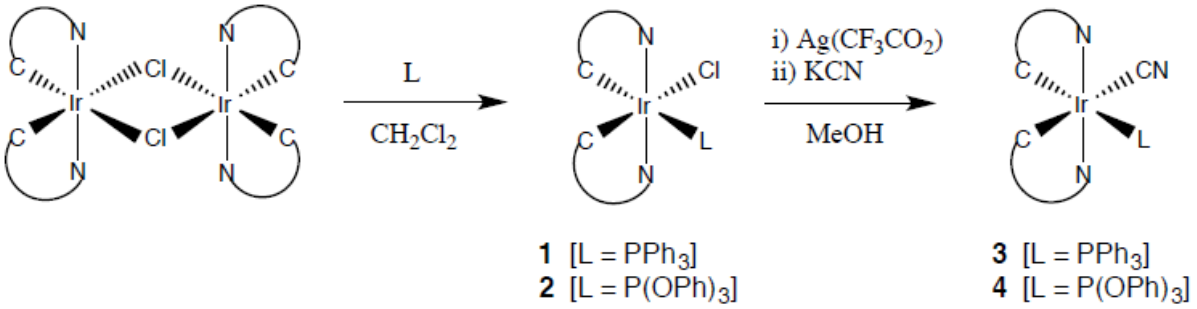

Results and Discussion

Synthesis and Structure. The reaction sequence is depicted in Scheme 1. Thus, cyclometalated dichloro-bridged iridium dimer $[(46dfppy)_2Ir(Cl)]_2$ was smoothly cleaved by phosphine or phosphite ligands in methylene chloride to yield the chloro monomers $Ir(46dfppy)_2(L)(Cl)$, where L=PPh_3 (**1**)[11] or $P(OPh)_3$ (**2**). The *trans*-N,N and *cis*-C,C bonding of the difluorophenylpyridine ligands about the iridium center is maintained upon addition of the monodentate phosphorus ligand (vide *infra*). Treatment of these chloro monomers with silver trifluoroacetate in methanol followed by potassium cyanide leads to replacement of the chloride ligand to form the cyano complexes $Ir(46dfppy)_2(L)(CN)$, where L=PPh_3 (**3**) or $P(OPh)_3$ (**4**), again with retention of geometry about the iridium. The chemical structures for the compounds under discussion are shown in Figure 1.

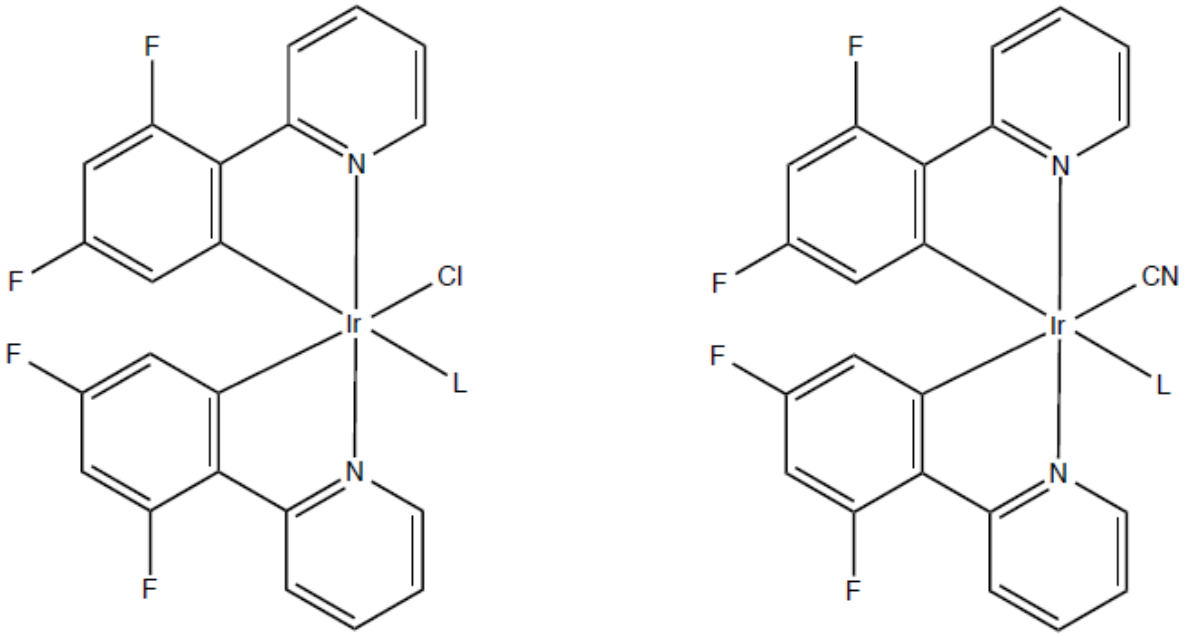

1 [L = PPh_3]
2 [L = $P(OPh)_3$]

3 [L = PPh_3]
4 [L = $P(OPh)_3$]

Figure 1. Chemical structures of compounds **1**, **2**, **3** and **4**.

The molecular structures of compounds **1**-**4** have been confirmed by x-ray crystallography and ORTEP diagrams of these complexes are shown in Figures 2-5; crystal and structure refinement data are provided in Table 1. All of the complexes exhibit the same distorted octahedral geometry: the pyridyl nitrogen atoms of the 46dfppy ligands are *trans* to each other while the phenyl carbon atoms bound to the iridium are *cis*. The phosphorus ligand and anionic ligand (Cl^- or CN^-) are both mutually *cis* to the pyridyl nitrogens as well as *cis* to each other. The octahedral symmetry around the iridium atom is distorted in that the non-phosphorus ligands are pushed away from the phosphorus ligands presumably due to steric factors. Thus the N-Ir-N bond angles (ideally 180°) are collapsed in all complexes, ranging from 167°-168°. In the chloride complexes the Cl-Ir-C bond angles are collapsed somewhat (172° and 174°) while in the cyanide complexes the C-Ir-C(N) angles are 171° and 174°. The phenyl and pyridine rings in each 46dfppy ligand are slightly twisted with respect to each other across the C-C bond linking the two rings. The dihedral angle between best planes for the two rings averages 5° in **1**,**2**, and **4** and 7.5° in **3**. There is a pronounced trans effect due to the phosphorus ligand. Thus, in **1**, the Ir-C bond length trans to the phosphine is 0.036 Å longer than the Ir-C bond trans to the chloride. The difference in **2** is even more pronounced with an elongation of 0.054 Å for the bond trans to the phosphite. This is in accord with Tolman's substituent effect parameter,[18] which is larger for OPh (9.7) compared to Ph (4.3) and is representative of the electronic effect of phosphorus ligands. For compounds **3** and **4** we are comparing Ir-C bond lengths trans to

phosphorus and cyanide ligands. In **3**, the Ir-C bond length trans to the phosphine is 0.016 Å longer than the Ir-C bond trans to the cyanide while in **4** the elongation for phosphite vs. cyanide is 0.021 Å. Note that the trans effect for the phosphorus ligand in the chloride complexes is more pronounced than in the cyanide complexes. This is reflective of the strong field cyanide ligand exerting its own trans effect in **3** and **4**. The iridium-phosphorus bonding can be compared directly by looking at the relevant bond lengths. Thus, the Ir-P bond in **2** (phosphite) is 0.14 Å shorter than in **1** (phosphine) while the same bond in **4** is 0.11 Å shorter than in **3**. While we cannot rule out steric factors due to the larger cone angle[14] of the phosphine (145°) compared to the phosphite (128°) (which would tend to elongate the Ir-phosphine bond), this data suggests at least some contribution from electronic factors resulting in reduced Ir-P bond lengths in phosphite (**2** and **4**) compared to phosphine (**1** and **3**) complexes. Two of the structures in this set have important crystallographic features to note. First, **1** crystallizes in space group $P2_1/n$ with two molecules in the asymmetric unit (Z=8, Z'=2). The centers of mass for both molecules are aligned along the *c*-axis in the same relative conformation. This suggests the structure could become modulated at some other temperature or could simplify to a related $P2_1/n$ Z'=1 structure at some elevated temperature. Second, **3** is a triple-solvate of methanol where all three solvent molecules are concatenated through hydrogen bonds originating on the cyanide nitrogen acceptor. The non-hydrogen atoms of the methanol solvent refined poorly such that C-O bond distances were restrained and these six atoms were refined with isotropic displacement parameters.

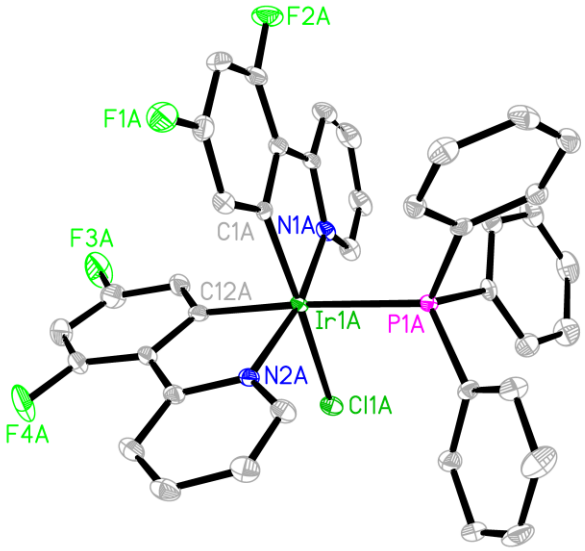

Figure 2. Thermal ellipsoid drawing of **1a** is presented at the 50% probability level with the hydrogen atoms omitted for clarity. Two molecules are found in the asymmetric unit; only molecule **A is** shown in the figure. Selected bond distances (Å) and bond angles (°) for **1a**: Ir1A-C1A 2.008(3), Ir1A-N1A 2.043(2), Ir1A-C12A 2.044(3), Ir1A-N2A 2.067(2), Ir1A-P1A 2.4415(6), Ir1A-Cl1A 2.4726(7), N1A-Ir1A-N2A 169.03(9), C12A-Ir1A-P1A 174.79(8), and C1A-Ir1A-Cl1A 172.31(8); for **1b**: Ir1B-C1B 2.009(3), Ir1B-C12B 2.039(3), Ir1B-N1B 2.043(2), Ir1B-N2B 2.065(2), Ir1B-P1B 2.4293(6), Ir1B-Cl1B 2.4642(7), N1B-Ir1B-N2B 168.25(9), C12B-Ir1B-P1B 174.48(8), and C1B-Ir1B-Cl1B 171.48(8).

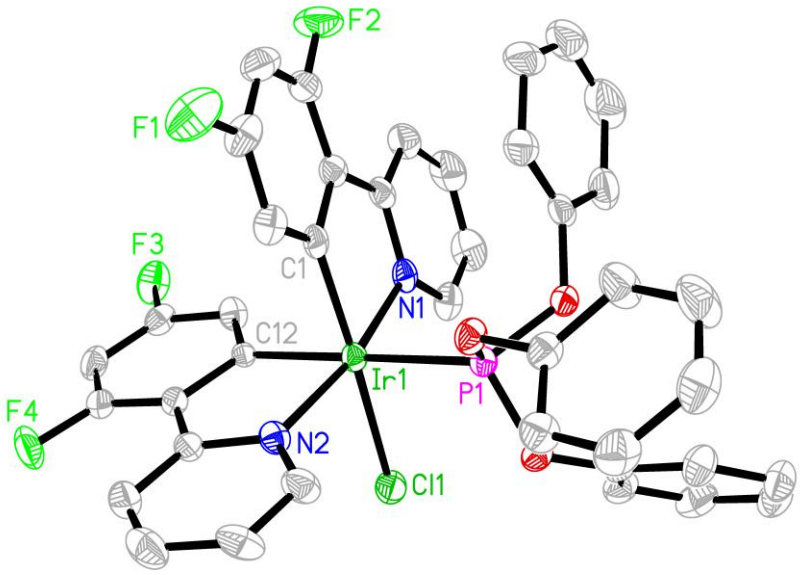

Figure 3. Thermal ellipsoid drawing of **2** is presented at the 50% probability level with the hydrogen atoms omitted for clarity. Selected bond distances (Å) and bond angles (°) for **2**:Ir1-C1 2.005(4), Ir1-N1 2.050(3), Ir1-C12 2.059(3), Ir1-N2 2.065(3), Ir1-P1 2.2979(9), Ir1-Cl1 2.4587(9), N1-Ir1-N2 168.44(11), C12-Ir1-P1 178.13(10), and C1-Ir1-Cl1 174.03(10).

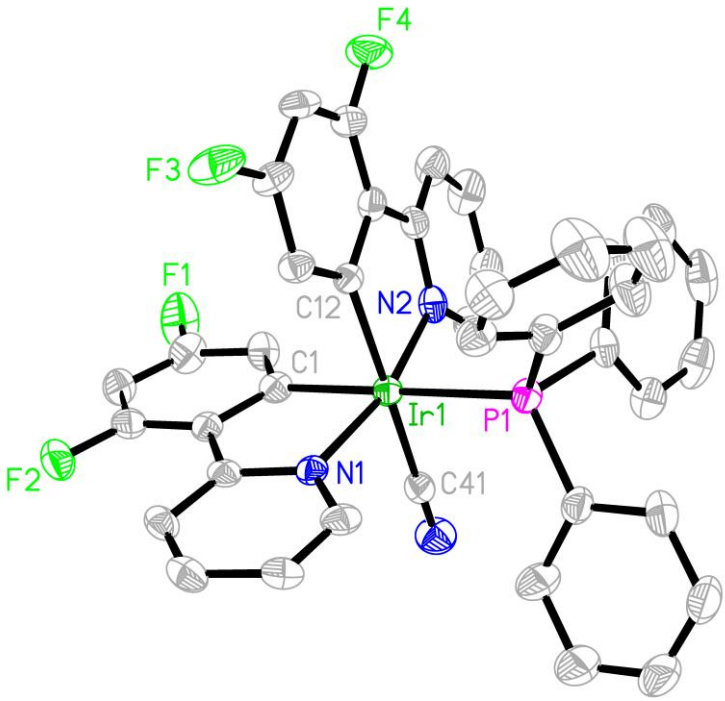

Figure 4. Thermal ellipsoid drawing of **3 · 3(CH3OH)** is presented at the 50% probability level with the hydrogen atoms and three methanol solvate molecules omitted for clarity. Selected bond distances (Å) and bond angles (°) for **3**: Ir1-C12 2.039(5), Ir1-C41 2.048(6), Ir1-C1 2.055(5),

Ir1-N1 2.058(5), Ir1-N2 2.068(4), Ir1-P1 2.4039(14), C41-Ir1-C1 171.3(2), N1-Ir1-N2 167.09(17), and C12-Ir1-P1 179.47(16).

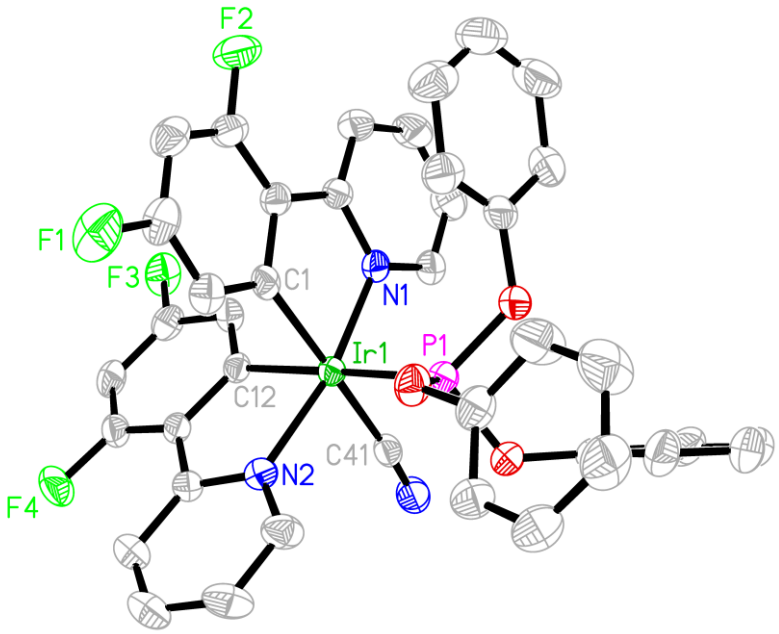

Figure 5. Thermal ellipsoid drawing of **4** is presented at the 50% probability level with the hydrogen atoms omitted for clarity. Selected bond distances (Å) and bond angles (°) for **4**: Ir1-C1 2.043(3), Ir1-N1 2.051(2), Ir1-C41 2.054(3), Ir1-C12 2.064(3), Ir1-N2 2.070(2), Ir1-P1 2.2924(7), C1-Ir1-C41 173.88(11), N1-Ir1-N2.167.61(9), and C12-Ir1-P1 178.28(8).

Table 1. Crystal data and structure refinement data for **1**, **2**, **3**, and **4**.

Identification code	**1**	**2**	**3** · 3(CH_3OH)	**4**
Empirical formula	$C_{40}H_{27}ClFIrN_2P$	$C_{40}H_{27}ClF_4IrN_2O_3P$	$C_{44}H_{39}F_4IrN_3O_3P$	$C_{41}H_{27}F_4IrN_3O_3P$
Formula weight	870.25	918.25	956.95	908.82
Temperature	123(2) K	173(2) K	123(2) K	173(2) K
Wavelength	1.54178 Å	0.71073 Å	0.71073 Å	1.54178 Å
Crystal system	Monoclinic	Triclinic	Monoclinic	Triclinic
Space group	$P2_1/n$	$P\bar{1}$	$P2_1/n$	$P\bar{1}$
Unit cell dimensions	*a* = 10.5528(3) Å	*a* = 10.3770(9) Å	*a* = 13.359(1) Å	*a* = 10.3157(2) Å
	b = 31.4059(8) Å	*b* = 11.5597(10) Å	*b* = 14.9094(11) Å	*b* = 11.5341(3) Å
	c = 19.6541(5) Å	*c* = 14.6959(12) Å	*c* = 20.1848(15) Å	*c* = 14.7501(4) Å
	α = 90°	α = 98.595(1)°	α = 90°	α = 98.0470(16)°
	β = 94.945(1)°	β = 91.502(1)°	β = 103.552(1)°	β = 91.5289(17)°
	γ = 90°	γ = 100.344(1)°	γ = 90°	γ = 99.6871(15)°
Volume	6489.5(3) $Å^3$	1712.2(3) $Å^3$	3908.4(5) $Å^3$	1710.67(7) $Å^3$
Z, Z'	8, 2	1, 1	4, 1	2, 1
Density (calculated)	1.781 Mg/m^3	1.781 Mg/m^3	1.626 Mg/m^3	1.764 Mg/m^3
Absorption coefficient	9.674 mm^{-1}	4.089 mm^{-1}	3.521 mm^{-1}	8.582 mm^{-1}
F(000)	3408	900	1904	892
Crystal color, morphology	Yellow, Plate	Yellow, Plate	Yellow, Block	Yellow, Prism
Crystal size	0.30 x 0.20 x 0.10 mm^3	0.35 x 0.22 x 0.08 mm^3	0.35 x 0.25 x 0.18 mm^3	0.12 x 0.05 x 0.05 mm^3
θ range	2.659 to 74.565°	1.813 to 27.593°	1.715 to 27.479°	3.030 to 68.341°
Reflections collected	81498	20305	45277	22361
Independent reflections	13061 [R_{int} = 0.0630]	7827 [R_{int} = 0.0463]	8951 [R_{int} = 0.0672]	6158 [R_{int} = 0.0326]
Observed reflections	10681	6706	6750	5688
Completeness	99.5%	99.8%	100.0%	98.8%
Absorption correction	Multi-scan	Multi-scan	Multi-scan	Multi-scan
Max. and min. transmission	0.2478 and 0.1129	0.7356 and 0.3287	0.5698 and 0.3721	0.5468 and 0.1531
Data / restraints / parameters	13061 / 0 / 883	7827 / 0 / 469	8951 / 3 / 475	6158 / 0 / 478
Goodness-of-fit on F^2	1.017	1.021	1.021	1.039
Final *R* indices [$I>2\sigma(I)$]	*R*1 = 0.0226, *wR*2 = 0.0470	*R*1 = 0.0315, *wR*2 = 0.0555	*R*1 = 0.0415, *wR*2 = 0.0993	*R*1 = 0.0209, *wR*2 = 0.0475
R indices (all data)	*R*1 = 0.0340, *wR*2 = 0.0503	*R*1 = 0.0402, *wR*2 = 0.0589	*R*1 = 0.0623, *wR*2 = 0.1095	*R*1 = 0.0245, *wR*2 = 0.0488
Largest diff. peak and hole	0.851 and -0.742 e.$Å^{-3}$	1.196 and -0.728 e.$Å^{-3}$	1.555 and -1.126 e.$Å^{-3}$	0.921 and -0.508 e.$Å^{-3}$

Spectroscopy. The UV-visible electronic absorption spectra of iridium complexes **3**, **4** and FIrpic in CH_2Cl_2 solution (Figure 6) are dominated by an intense absorption band at ~260 nm (ε =30- 40 × 10^3 M^{-1} cm^{-1}) assigned to spin-allowed ligand centered (LC) $^1(\pi-\pi^*)$ transitions on the cyclometallated ligand. The weaker bands at lower energies (300–440 nm) have charge-transfer (CT) character related to electronic transitions from the metal center to the cyclometallated ligands (MLCT). The absorption spectra shown in Figure 6 suggest that the ^{1}MLCT state lies at 413 nm (**3**) or 409 nm (**4**), while the ^{3}MLCT state lies at 441 nm (**3**) or 437 nm (4). These bands exhibit very low relative absorption, and reveal higher lying T_1 states for these complexes, compared to the 455 nm band of

FIrpic. This is presumably due to the substitution of the picolinate ligand in FIrpic by the stronger field cyano and phosphine (compound **3**) or phosphite (compound **4**) ligands. These stronger field ligands stabilize the metal-centered HOMO. In addition, the phosphite causes a slightly larger blue shift of the absorption bands than the phosphine as could be predicted from the electronic effects shown in the molecular structure (vide supra).

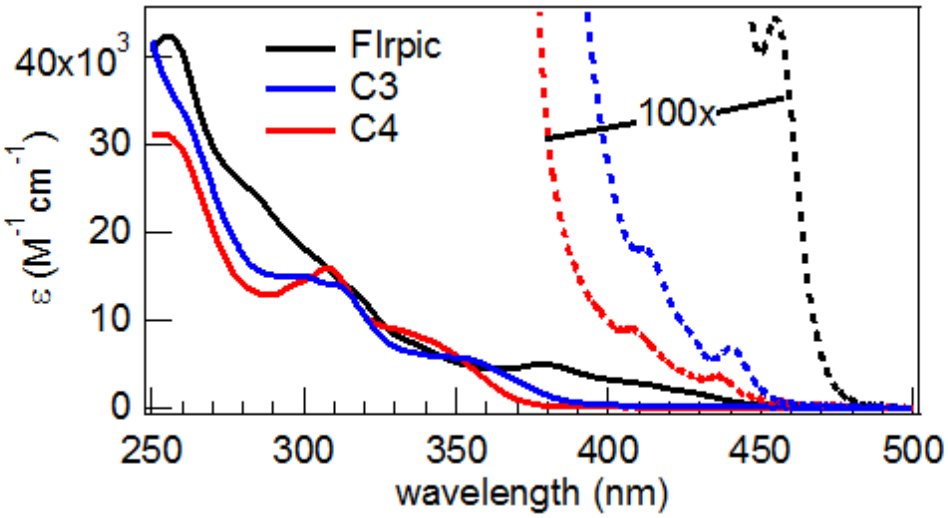

Figure 6. UV-visible absorption spectra of the three iridium complexes in CH_2Cl_2 solution. Spectra were acquired with 10^{-5} M solutions (left, solid lines) and 10^{-4} M solutions (right, dashed lines). The spectra acquired with 10^{-4} M solutions were additionally scaled by 10x in order to show the weak ^{1}MLCT and ^{3}MLCT bands.

The emission, thought to be principally phosphorescence for all three compounds, shown in Figure 7 reveal significantly blue-shifted spectra for **3** and **4**, compared to FIrpic. As expected from the absorption spectra, the phosphite compound **4** is blue-shifted from the phosphine compound **3**. Table 2 lists the several measured properties of **3** and **4**, in comparison to FIrpic. Table 3 shows that the phosphorescence quantum yields for **3** and **4** are high, about 80%, and their measured decay times, 4.5 and 2.9 μs, respectively, are longer than that measured for FIrpic, at 1.2 μs. The higher-lying T_1 states for **3** and **4**, compared to FIrpic requires an OLED or scintillation host with an even higher lying T_1 state, such as mCP. The CIE coordinates were calculated to be (x = 0.16, y = 0.24) and (x = 0.16, y = 0.21) for **3** and **4**, respectively. These values indicate considerably blue emission compared to FIrpic (x = 0.16, y = 0.33), and they approach the desirable "true blue" emission, in the CIE coordinate range (x < 0.2, y < 0.2).

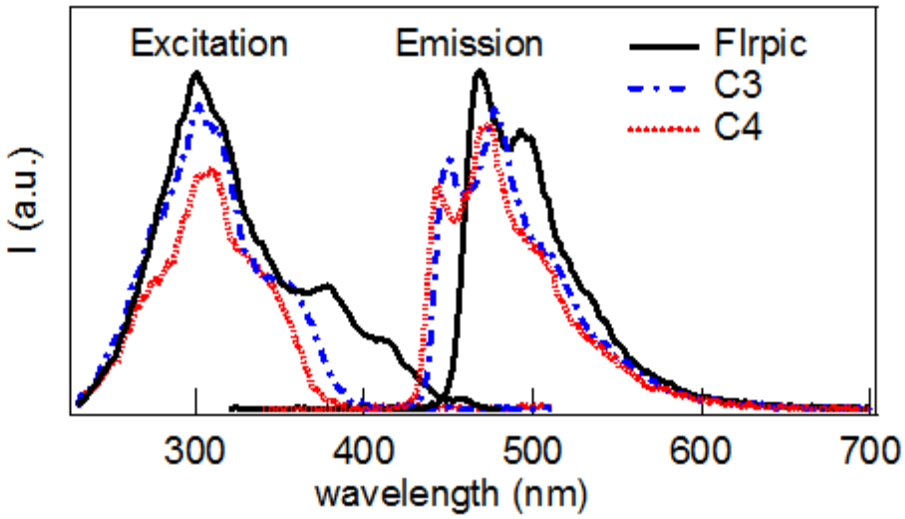

Figure 7. Excitation (λ_{em} = 520 nm) and photoluminescence (λ_{ex} = 310 nm) emission spectra acquired with 10^{-5} M solutions in CH_2Cl_2 of the three iridium compounds show the blue shifted emission of **3** and **4**, compared to FIrpic.

Table 2. Absorption peaks (λ_{max} for each feature) and their extinction coefficients for the three iridium compounds in CH_2Cl_2 solution.

	λ_1 (nm); ε_1 (M^{-1} cm^{-1})	λ_2 (nm), ε_2 (M^{-1} cm^{-1})	λ_3 (nm), ε_3 (M^{-1} cm^{-1})	λ_4 (nm); ε_4 (M^{-1} cm^{-1})	λ_5 (nm), ε_5 (M^{-1} cm^{-1})	λ_6 (nm), ε_6 (M^{-1} cm^{-1})
C3	255; 37,050	298; 15,100	312; 13,900	355; 5560	413; 170	441; 65
C4	255; 31,100	296; 14,000	308; 16,000	345; 7060	408; 85	436; 35
FIrpic	255; 42,350	309; 15,900	320; 12,100	339; 6,900	379; 4,970	455; 430

Table 3. Physical properties of the three iridium complexes in CH_2Cl_2 solution. Lowest triplet energy, T_1, was estimated from the absorption spectra shown in Figure 6.

	Φ_{PL}	τ_P (μs)	PL, λ_{max} (nm)	T_1 (eV)
C3	0.82	4.5	451, 478	2.81
C4	0.81	2.9	443, 471	2.84
FIrpic	0.60	1.2	468, 493	2.73

Conclusions

A series of bis-cyclometallated iridium phosphine and phosphite complexes has been synthesized containing either chloro or cyano ligands. All of the compounds have been characterized by x-ray crystallography; bond length data show that the phosphorus ligands

exert a trans effect. The emissive cyano compounds have been studied by optical spectroscopy. We have demonstrated that replacement of the picolinate ligand in FIrpic by the combination of cyano and phosphorus ligands results in a blue shift of the emission with enhanced fluorescence quantum yield. The blue shift in emission is presumably due to the stabilization of the metal-centered HOMO by the strong field cyano and phosphorus ligands. Greater stabilization and higher energy emission is found for the phosphite ligand relative to the phosphine.

Experimental Section

Equipment. Optical absorption spectra were obtained with a Thermo Evolution 220 UV-visible spectrometer, and emission spectra were measured with a Thermo Lumina fluorescence spectrometer. Phosphorescence lifetime measurements were acquired using a flashlamp-pumped Nd:YAG laser at 266 nm with 20 ns pulses. Luminescence was collected with a monochromator coupled to an R928 Hamamatsu PMT and read out by an oscilloscope. Quantum efficiency measurements were carried out at room temperature in degassed methylene chloride solvent. NMR spectra were recorded on a Bruker Avance III 600 MHz spectrometer.

X-ray Crystallography. Suitable crystals for **1**, **2**, **3**, and **4** were selected for single-crystal diffraction studies. Specimens **1** and **4** were mounted on a Bruker-AXS VENTURE Diffractometer with a CuKα IμS microfocus source (λ = 1.54178 Å) and PHOTON-100 (CMOS) detector. Specimens **2** and **3** were mounted on a BRUKER-AXS SMART Diffractometer with a MoKα normal-focus tube source with a pyrolytic graphite monochromator (λ = 0.71073 Å) and an APEX-II (CCD) detector. Unit cell constants were determined initially with the APEX-II software. Final unit cell constants were calculated on large sets of strong reflections from the integration of all data with SAINT. A multi-scan scaling and absorption correction were applied with SADABS based on the Laue class determined for each crystal structure. The crystal structures were solved by direct methods using SHELXL-97 or SHELXT-2014. Final least-squares refinements were completed with SHELXL-2014. All non-hydrogen atoms were refined with anisotropic displacements, except for **3** (see discussion section). Hydrogen atoms were placed as riding atoms at calculated positions with isotropic displacements relative to respective host atoms. Crystallographic data is summarized in Table 1A. CIF data is available from the CCDC with deposit numbers: **1** XXXXXX, **2** XXXXXX, **3** XXXXXX, and **4** XXXXXX.

Synthesis. The compounds $[(46dfppy)_2Ir(Cl)]_2$[14] and $(46dfppy)_2Ir(PPh_3)(Cl)$[17] were prepared by the literature methods.

$(46dfppy)_2Ir[P(OPh)_3](Cl)$ (Compound 2). 2.5 g (2.05 mmol) of $[(dfppy)_2Ir(Cl)]_2$ and 1.47 g (4.7 mmol) of $P(OPh)_3$ were combined in 225 mL nitrogen-purged methylene chloride and the solution was stirred overnight at room temperature under nitrogen. The solvent was removed under vacuum to provide the crude product as a yellow powder. This material was flash chromatographed on a silica column using dichloromethane eluent. The eluted material was concentrated and cooled in the freezer to obtain 3.2 g of yellow crystalline product (85% yield). Anal. Calcd for $IrC_{40}H_{27}N_2ClF_4O_3P$: C, 52.32; H, 2.96; N,

3.05. Found: C, 52.38; H, 3.22; N, 2.99. ^{1}H NMR (600 MHz, $CDCl_3$) (ppm): 9.71 (d, J=5.6 Hz, 1H), 9.52 (d, J=5.7 Hz, 1H), 8.34 (d, J=8.0 Hz, 1H), 8.13 (d, J=8.3 Hz, 1H), 7.86 (t, J=7.6 Hz, 1H), 7.73 (t, J=7.6 Hz, 1H), 7.13 (m, 7H), 7.05 (m, 3H), 6.98 (t, J=6.6 Hz, 1H), 6.78 (m, 6H), 6.39 (t, J=10.8 Hz, 1H), 6.32 (t, J=10.3 Hz, 1H), 5.67 (d, J= 8.5 Hz, 1H), 5.24 (t, J=9.1 Hz, 1H). ^{19}F NMR (564 MHz, $CDCl_3$) (ppm): -107.16 (quintet, J=9.7 Hz, 1F), -107.56 (q, J=9.0 Hz, 1F), -109.52 (q, J=11.9 Hz, 1F), -110.65 (t, J=11.1 Hz, 1F).

(46dfppy)$_2$Ir(PPh$_3$)(CN) (Compound 3). 1.43 g (1.64 mmol) of (dfppy)$_2$Ir(PPh$_3$)(Cl) was dissolved in 150 mL methanol and heated to 50 °C. Silver trifluoroacetate was added and the resultant silver chloride was filtered off on a celite pad. Potassium cyanide (0.20 g, 3.08 mmol) dissolved in 20 mL of methanol was added to the filtrate and this solution was refluxed for 1 hour under nitrogen. The reaction mixture was concentrated and cooled in the freezer. The resultant yellow crystals were collected and washed with cold methanol to yield 0.75 g of product. A second crop of 0.40 g crystals was collected by concentrating and cooling the filtrate and washings. This second batch showed NMR results identical to the first batch for a combined yield of 81%. Anal. Calcd for IrC41H27N3F4P: C, 57.20; H, 3.16; N, 4.88; F, 8.83; P, 3.60. Found: C, 56.0; H, 2.87; N, 5.07; F, 8.92; P, 3.40. ^{1}H NMR (600 MHz, $CDCl_3$) (ppm): 9.07 (d, J=5.7Hz, 1H), 8.67 (d, J=5.6 Hz, 1H), 8.37 (d, J=6.5 Hz, 1H), 8.06 (d, J=8.4 Hz, 1H), 7.81 (t, J=7.7 Hz, 1H), 7.60 (t, J=7.7 Hz, 1H), 7.33 (m, 9H), 7.22 (m, 6H), 6.79 (t, J=6.3 Hz, 1H), 6.69 (t, J=6.3 Hz, 1H), 6.41 (m, 2H), 5.38 (m, 2H). ^{19}F NMR (564 MHz, $CDCl_3$) (ppm): -106.98 (quintet, J=8.4 Hz, 1F), -108.07 (q, J=8.9 Hz, 1F), -109.73 (m, 2F).

(46dfppy)$_2$Ir[P(OPh)$_3$](CN) (Compound 4). The same procedure as described for (46dfppy)$_2$Ir(PPh$_3$)(CN) was followed, giving yellow crystals in 65% yield. Anal. Calcd for IrC41H27N3F4O3P: C, 54.18; H, 2.99; N, 4.62. Found: C, 53.52; H, 3.03; N, 4.68. ^{1}H NMR (600 MHz, $CDCl_3$) (ppm): 9.50 (d, J=5.6 Hz, 1H), 9.40 (d, J=5.7 Hz, 1H), 8.35 (d, J=7.9 Hz, 1H), 8.17 (d, J=8.6 Hz, 1H), 7.88 (t, J=7.8 Hz, 1H), 7.76 (t, J=7.8 Hz, 1H), 7.15 (m, 7H), 7.07 (m, 3H), 6.91 (t, J=6.6 Hz, 1H), 6.83 (m, 6H), 6.41 (t, J=10.6 Hz, 1H), 6.30 (t, J=10.1 Hz, 1H), 5.56 (d, J=7.4 Hz, 1H), 5.30 (t, J=7.8 Hz, 1H). ^{19}F NMR (564 MHz, $CDCl_3$) (ppm): -107.10 (quintet, J=9.7 Hz, 1F), -107.60 (q, J=8.9 Hz, 1F), -109.46 (q, J=11.9 Hz, 1F), -110.07 (t, J=10.9 Hz, 1F).

Acknowledgements

We thank the X-Ray Crystallographic Laboratory, LeClaire-Dow Instrumentation Facility, Department of Chemistry, University of Minnesota for its contribution. The authors would like to acknowledge Ms. Laura Clouston and the CHEM5755 X-Ray Crystallography for the assistance in collecting single crystal diffraction data on sample **1**. The Bruker-AXS D8 Venture diffractometer was purchased through a grant from NSF/MRI (#1229400) and the University of Minnesota. This work was funded by the National Nuclear Security Administration, Defense Nuclear Nonproliferation Research and Development Office of the U.S. Department of Energy under Contract DE-AC03-76SF00098, and was performed under the auspices of the U. S. Department of Energy by Lawrence Livermore National Laboratory under Contract DE-AC52-07NA27344.

Appendix A. Supplementary data

CIF files and structural drawings with complete atom labeling for **1-4** can be found at:

References

[1] L. Flamigni, A. Barbieri, C. Sabatini, B. Ventura, F. Barigelletti, Top. Curr. Chem., 281 (2007) 143-203.

[2] J.H. Seo, S.C. Lee, Y.K. Kim, Y.S. Kim, Thin Solid Films, 517 (2009) 4119-4121.

[3] Y. Zhang, Y. Xu, Q. Niu, J. Peng, W. Zang, X. Zhu, Y. Cao, J. Mater. Chem., 17 (2007) 992-1001.

[4] S. Lamansky, P. Djurovich, D. Murphy, F. Abdel-Razzaq, R. Kwong, I. Tsyba, M. Bortz, R. Bau, M.E. Thompson, Inorg. Chem., 40 (2001) 1704-1711.

[5] Y.-M. Wang, F. Teng, L.-H. Gan, H.-M. Liu, X.-H. Zhang, W.-F. Fu, Y.-S. Wang, X.-R. Xu, J. Phys. Chem. C, 112 (2008) 4743-4747.

[6] L. Ziao, Z. Chen, B. Qu, J. Luo, Sh. Kong, Q. Gong, J. Kido, Adv. Mater., 23, (2011) 926–952.

[7] B.L.Rupert, N.J. Cherepy, B.W. Sturm, R.D. Sanner, S.A. Payne, Europhysics Lett., 97, (2012) 22002.

[8] K. Dedian, J. Shi, E. Forsythe, D.C. Morton, P.Y. Zavalij, Inorg. Chem., 46, (2007) 1603-1611.

[9] X. Shen, X.-H. Hu, F.-L. Wang, F. Sun, Y.-Q. Yang, Y. Xu, S. Chen, D.-R. Zhu, Inorg. Chem Commun. 13 (2010) 1096-1099.

[10] C.-H. Hsieh, F.-I. Wu, C.-H. Fan, M.-J. Huand, K.-Y. Lu, P.-Y. Chou, Y.-H. Ou Yang, S.-H. Wu, I.-C. Chen, S.-H. Chou, K.-T. Wong, C.-H. Cheng, Chem. Eur. J., 17, (2011), 9180-9187.

[11] J.-B. Kim, S.-H. Han, K. Yang, S.-K. Kwon, J.-J. Kim, Y.-H. Kim, Chem. Commun., 51 (2015), 58.

[12] E. Baranoff and B.F.E. Curchod, Dalton Trans. (2015) in press.

[13] Md. K. Nazeeruddin, R. Humphry-Baker, D. Berner, S. Rivier, L. Zuppiroli, M. Graetzel, J. Am. Chem. Soc. 125 (2003) 8790-8797.

[14] A.B. Tamayo, B.D. Alleyne, P.I. Djurovich, S. Lemansky, I. Tsyba, N.N. Ho, R. Bau, M.E. Thompson, J. Amer. Chem. Soc. 125 (2003) 7377-7387.

[15] J. Brooks, Y. Babayan, S. Lamansky, P.I. Djurovich, I. Tsyba, R. Bau, M.E. Thompson, Inorg. Chem. 41 (2002) 3055-3066.

[16] X. Shen, H. Yang, X.-H. Hu, Y. Xu, F.-L. Wang, S. Chen, D.-R. Zhu, Inorg. Chem. Commun. 12 (2009) 785-788.

[17] C.-L. Lee, R.R. Das, J.-J. Kim, Curr. Appl. Phys. 5 (2005) 309-313.

[18] C.A. Tolman, Chem. Rev. 77 (1977) 313-348.

[19] Y. You, S.Y. Park, J. Amer. Chem. Soc. 127 (2005) 12438-12439.